

# COMPUTATIONAL BINDING STUDIES FOR HOST-GUEST INTERACTION OF MOSCS

Dr. Anila Ishaque<sup>1</sup>, Dr. Muhammad Waqas Rana<sup>2</sup>, Dr. Muhammad Bilal Ikram<sup>3</sup>

<sup>1</sup> Fatima Jinnah Medical University, Lahore, Pakistan

<sup>2</sup> Demonstrator at AJK Medical College, Muzaffarabad Azad Kashmir, Pakistan

<sup>3</sup> Sharif Medical & Dental College, Lahore, Pakistan

**Abstract:** Through simple models, host-guest interactions of biologically relevant molecules non-covalently binding to the building blocks (serving as simplified models) of metal-organic super containers (MOSCs) were determined using ab initio density functional theory and molecular dynamics analysis of both host and guest molecules. Binding sites were chosen by qualitatively analyzing electrostatic potential maps. Multiple host-guest orientations were explored, to determine preferred binding locations on the MOSC. Dipole-dipole interactions are primarily responsible for the mutual attraction or repulsion of these molecules.

**Keywords:** metal-organic super container, host-guest, binding study

## Introduction

Metal-organic super containers (MOSCs)<sup>6</sup> represent a new class of biomimetic container molecules. MOSCs allow for varied geometric placements of the “building blocks” which permits a highly modular design. Three types of such building blocks include (a) sulfonycalix[4]arenes<sup>7</sup> (SC) shown in **Figure 1(a)**, (b) tetranuclear complexes (TNCs), shown in **Figure 1(b)**, which consist of a SC bound to four  $M^{2+}$  ions furnished by four carboxylate groups, and  $\mu_4$  oxygen,<sup>8</sup> and (c) various carboxylate linkers shown in **Figure 1(c)**.

An example of the complete MOSC is represented in form of a schematic diagram, in **Figure 1(e)** and in form of atomistic model, in **Figure 1(f)**. Each super container possesses multiple internal and external cavities and has variable geometry depending upon the selection of the carboxylate building blocks. It is in part because of their tunable character that MOSCs can be utilized in a wide range of applications, including drug delivery and biomedical sensing.

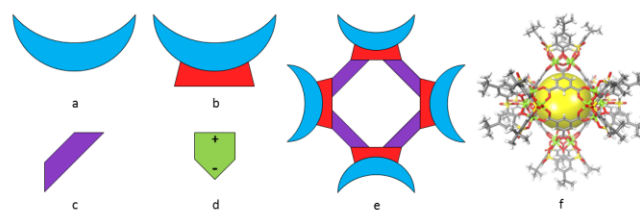


Figure 1 Structural details of MOSC building blocks

Cartoon diagram of the ‘building blocks’ of a MOSC. a) sulfonycalix[4]arene, b) tetranuclear complex, c) carboxylate linkages, d) aspirin. Note that aspirin is a polar molecule, as indicated by a plus and minus sign at opposite ends of the shape. e) Cartoon diagram depicting a simplified MOSC structure to aid the reader in visualizing the super container molecule, and f) Example of a molecular structure of a MOSC.<sup>6a</sup> The yellow sphere aids in guiding the reader’s eyes in visualizing the MOSC’s three-dimensional shape.

Another class of materials closely related to the MOSCs are metal organic frameworks (MOFs). MOFs are a family of two-dimensional (2D) or three-dimensional (3D) infinite crystalline lattices formed from the combination of organic molecules connected to metal ions

or metal ion clusters.<sup>9</sup> Commonly, the organic molecules, known as linkers, are of a semi-rigid or rigid construction and form links between the metal ion clusters.<sup>10</sup> This design works in the same manner as scaffolds or similar frameworks, hence the name. Unfortunately, the exceedingly large number of atoms in an asymmetric unit of a typical MOF makes computational studies of these systems rather challenging.<sup>11</sup> This problem is present in MOSC systems as well. To reduce computational expense, we model properties of the chemically representative fragments of a MOSC system.

As is often done when studying MOFs, we model only parts of the system.<sup>12</sup> Considering the size of these MOSCs can approach the threshold of computational capabilities (at 200-800 atoms), we applied a 'divide and conquer' strategy and theoretically investigated the building blocks for these super-

containers. In computationally analyzing these molecules, we hope to better understand their binding capabilities and selectivity to guest molecules, in addition to fully understanding the characteristics of the binding sites.

Experimentally, these MOSCs were found to selectively and reversibly bind cationic guests, such as methylene blue dye.<sup>6b, 6c</sup> Utilizing ratiometric results from UV-Vis titrations of varying amounts of host and guest molecules revealed that SC and TNC bound two molecules of aspirin each. A MOSC, constructed from tert-butyl-sulfonylcalix[4]arene, 1,4-benzene-dicarboxylate linkers and cobalt(II), was found to bind more than thirty molecules of aspirin.<sup>6c</sup> It was this fifteen-fold increase in aspirin molecule adsorption that led to this study. In order to simplify our model, we have removed the tert-butyl groups and have assumed the conformation of SC is a rigid cup-shaped molecule,<sup>13</sup> which matches the shape of the TNC molecule, as TNC is held in the cup shape by the coordination of the metal ions with carboxylate groups, sulfonyl oxygens, and  $\mu$ -4-oxygen.

We explore the binding pattern of hosts (SC, TNC) and guest, as a function of 1) binding site, 2) relative

orientation (of their dipoles), and 3) distance between them (Figure 2).

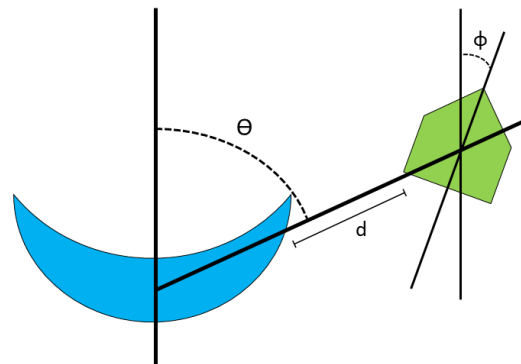


Figure 2 Diagram of mutual orientation of host and guest

Schematic diagram depicting the mutual spatial configurations of host (blue moon) and guest (green pentagon) can be approximately parameterized by three elements: 1) angle  $\Theta$  = direction, from which the guest approaches host (specifies the binding site), 2) angle  $\phi$  = determines mutual orientation of electrostatic dipoles of host and guest, and 3) distance  $d$  = between host and guest

## Methods

X-ray crystallographic data<sup>6a</sup> was used to obtain structural information for the cobalt-containing TNC, instead of running optimization, which gives us an exact correlation between experimental and computational work. Atomic structure determines initial positions of each ion,

$\vec{R}_i$ , in the model. The presence of transition metal ions provides a challenge for force field molecular mechanics approaches. Some existing force fields do not account for electronic polarization of the environment, an effect that can significantly reduce electrostatic interactions of partial atomic charges.<sup>14</sup> The force fields that do account for electronic polarization are too time-consuming for our project. Density-functional theory (DFT) was chosen because it offers the best balance between necessary computational time and accuracy. The main equation is the Kohn-Sham

equation, which is the Schrödinger equation of a fictitious system of non-interacting particles (typically electrons) that generate the same density as any given system of interacting particles.

$$\left( -\frac{\hbar^2}{2m} \nabla^2 + v[\rho(\mathbf{r})] \right) \phi^{KS}(\mathbf{r}) = \varepsilon_i \phi^{KS}(\mathbf{r}) \quad (1)$$

Here the first term corresponds to kinetic energy  $T$  and uses symbol of gradient  $\nabla = \left( \frac{\partial}{\partial x}, \frac{\partial}{\partial y}, \frac{\partial}{\partial z} \right)$ .

In solving equation (1) one finds a set of one-electron orbitals  $\phi^{KS}(\mathbf{r})$ , and their energies  $\varepsilon_i$ . The orbitals are combined with orbital occupation function  $f_i$  for constructing the total density of electrons

$$\rho(\mathbf{r}) = \sum_{i \leq \text{HO}} f_i \phi^{KS}(\mathbf{r}) \phi^{KS}(\mathbf{r}) \quad (2)$$

The total density determines the potential

$$v[\rho(\mathbf{r})] = \frac{\delta}{\delta \rho} (E^{tot}[\rho] - T), \quad (3)$$

which is defined as the functional derivative of the total energy  $E^{tot}[\rho]$  minus kinetic energy  $T$  in respect to variation of the total density  $\rho(\mathbf{r})$  and includes interactions of electrons with ions, and three electron interactions: Coulomb, correlation, and exchange. Rectangular brackets symbolize a functional. Equations (1)-(3) are solved in the iterative, self-consistent manner. Electrostatic potential introduced in Eq. (3) illustrates interaction of a valence electron with background charge of electrons and ions. This electrostatic potential is a byproduct computed in DFT and several other methods.<sup>15</sup>

The electronic density of states (DOS) describes the number of states per interval of energy. We use DOS in order to characterize electronic structure of the studied models. DOS was defined as

where the Dirac delta function was approximated by

$$n(\varepsilon) = \sum_i \delta(\varepsilon - \varepsilon_i) \quad (4)$$

finite width Gaussian function and  $\varepsilon_i$  are the energies of a given KS orbital (calculated using DFT), and the index  $i$  runs over all orbitals calculated.

ESP maps are a three-dimensional representation of the charge distribution to visualize regions of a molecule with variable charge. Single point energy calculations were run on structures after geometry optimization. Binding energies of the host and guest were calculated using the equation:

$$E_{(bind)} = E_{(host+guest)}^{tot} - E_{(host)}^{tot} - E_{(guest)}^{tot} \quad (5)$$

Each molecule's ground-state energy was determined separately. Computed values of binding energy are compared to thermal quantum  $k_B T$  and to the energy of hydrogen bond in water.

## Results and Discussion

We used Gaussian 09 software to find an electronic structure with density functional theory.<sup>16</sup> We used this software to solve self consistent DFT equations. DFT with B97 dexchange- correlation functional and 6-311G(d) and LanL2DZ basis sets (for light elements and transition metals, respectively) in Gaussian software provides spatial electron density distributions for the ground state and for Kohn-Sham orbitals. Gauss View 5 was used as an interface for model- building and visualization of results.<sup>17</sup> Determination of the energy of the molecular systems was completed using the B97d functional, which includes a dispersion correction.<sup>18</sup> The B3LYP functional was used to generate electrostatic potential maps.

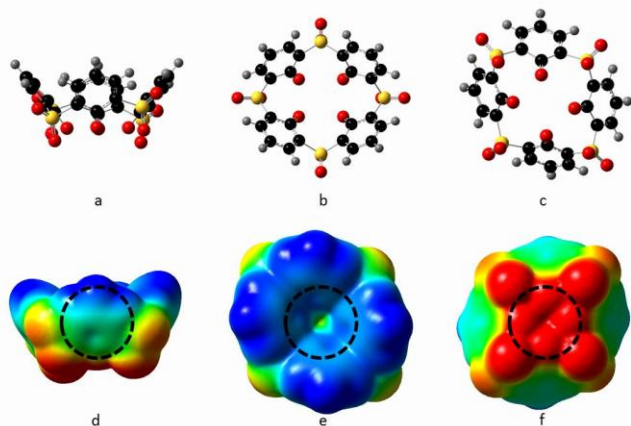


Figure 3 Sulfonylcalixarene models and ESP maps

Ball and stick models of sulfonylcalix[4]arene a) side view, b) top view, c) bottom view. Atom colors: black=carbon, red=oxygen, yellow=sulfur, grey=hydrogen. Electrostatic potential maps of sulfonylcalix[4]arene e) side view, f) top view, g) bottom view. Blue regions designate relative positive charge, transitioning into negative, indicated by red. The dotted black circles identify the binding locations we have chosen.

#### *Electrostatic Potential Maps*

Understanding the variable electron density of the hosts and guests was essential in determining possible binding sites. In order to do so, electrostatic potential (ESP) maps were generated, according to Eq. (3).<sup>15</sup> From these maps, we have identified the top ( $\Theta=0^\circ$ ), side ( $\Theta=90^\circ$ ), and bottom ( $\Theta=180^\circ$ ) of each host molecule as candidate sites (**Figures 3, 4**) due to either positive or negative regions existing on the surface of the molecule.<sup>19</sup> In SC, positive regions exist on the top of the molecule, with negative regions on the bottom. TNC shares these features, only to a greater extent, as the metals now draw even more electron density away from the top side of the molecule. ESP map of aspirin, shown in **Figure 5** allows selection of the mutual orientation of host and guest.

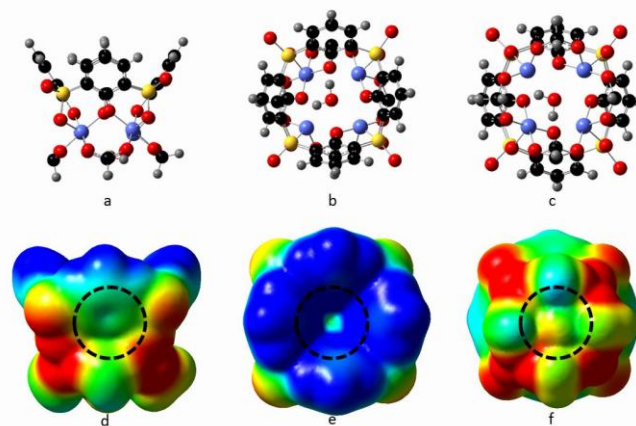


Figure 4 TNC models and ESP maps

Ball and stick models of the tetranuclear complex a) side view, b) top view, c) bottom view. Atom colors: black=carbon, red=oxygen, yellow=sulfur, blue=cobalt, grey=hydrogen. Electrostatic potential maps of the tetranuclear complex e) side view, f) top view, g) bottom view. Blue regions designate relative positive charge, transitioning into negative, indicated by red. The dotted black circles identify the binding locations we have chosen.

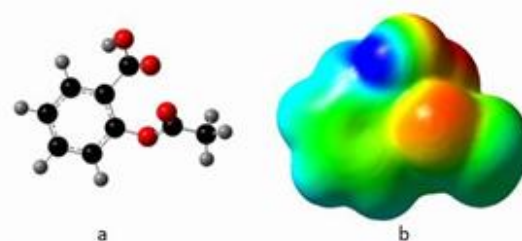


Figure 5 Aspirin model and ESP map

a) Ball and stick model of aspirin side view. Atom colors: black=carbon, red=oxygen, grey=hydrogen. b) Electrostatic potential map of aspirin, side view. Blue regions designate relative positive charge, transitioning into negative, indicated by red.

### Binding Studies

Each guest molecule was placed near the host, at  $d=3, 5, 7$  Angstroms from the host molecule.<sup>20</sup> We expect that a host-guest complex which displays stabilization will have a negative binding energy according to Eq. (5).<sup>21</sup> In addition, the guest, i.e. aspirin, has been placed in the direction of the host at two orientations: positive and negative dipole attacks with an example shown in **Figure 6**. In a positive dipole

attack, the benzene ring is close to the host molecule, whereas in the negative dipole attack the oxygen molecules are nearest to the host. These two positions were chosen because both the host and guest molecules have partially positive and partially negative regions.

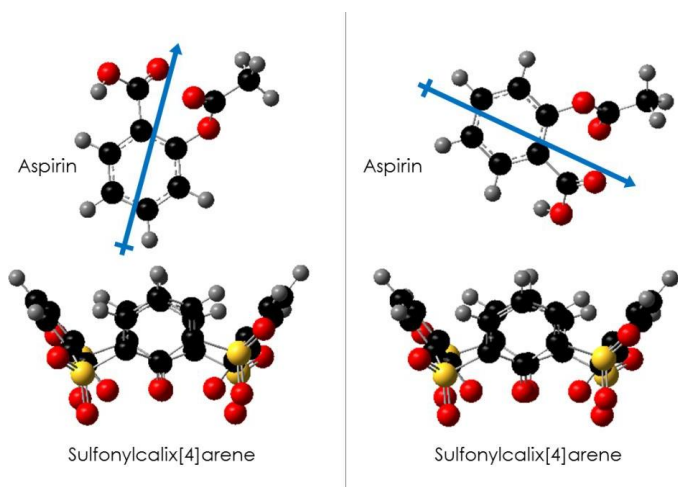


Figure 6 Two orientations of host and guest

Examples of various mutual orientations of host and guest molecules. Right: Scheme displaying the negative dipole attack orientation of the aspirin molecule in relation to the host, sulfonylcalix[4]arene. Note that a true ‘head-on’ orientation was not used due to the steric hindrance of the methane group on the aspirin molecule. Left: Scheme displaying the positive dipole attack orientation of the aspirin molecule in relation to the host, sulfonylcalix[4]arene.

**Tables 1 and 2** summarize the calculated binding energies. Binding energies exhibit clear dependence upon mutual orientation parameters  $\Theta$ ,  $\phi$ , and  $d$ . Binding energies decrease with increasing host-guest distance, with two exceptions: 1) SC, positive dipole attack from the top, and

2) TNC, positive dipole attack from the top. We consider the possibility that as the positive dipole of the aspirin approaches the top of the hosts (which are positively charged at that binding site), the guest experiences repulsion. Once the aspirin is displaced, there is a slight attraction between the molecules. The decrement of  $E(\text{bind})(d)$  with distance is attributed to several interaction mechanisms: Coulombic, <sup>1</sup>, dipole-

dipole <sup>1</sup>, etc.<sup>22</sup> Both host molecules, SC and TNC, provided,  $d^3$  favorable adsorption, but do so with an opposite dependence on angle. SC and TNC both prefer a negative dipole attack from the top and a positive dipole attack from the bottom. Some areas do not participate in binding, indicated by a positive value in the table, which corresponds to repulsion of species.

Table 1 Sulfonylcalixarene binding energies

Aspirin to sulfonylcalix[4]arene binding energies in eV as a function of structural parameters  $\phi$ ,  $\Theta$ , and  $d$ .

Table 1 Sulfonylcalixarene binding energies

Aspirin to sulfonylcalix[4]arene binding energies in eV as a function of structural parameters  $\phi$ ,  $\Theta$ , and  $d$ .

Orientation	$\phi$	Site	$\Theta$	3Å	5Å	7Å
Positive	0°	Top	0°	-0.171	-1.540	-1.444
	90°	Side	90°	-1.696	-1.537	-1.500
Dipole	180°	Bottom	180°	-1.915	-1.575	-1.519
Negative	180°	Top	0°	-1.813	-1.593	-1.512
	270°	Side	90°	-1.778	-1.510	-1.458
Dipole	0°	Bottom	180°	-1.544	-1.459	-1.462

Table 2 TNC binding energies

Aspirin to tetranuclear complex binding energies in eV as a function of structural parameters  $\phi$ ,  $\Theta$ , and  $d$ .

Orientation	$\phi$	Site	$\Theta$	3Å	5Å	7Å
Positive	0°	Top	0°	0.013	-0.058	0.023
	90°	Side	90°	0.440	0.446	0.450
Dipole	180°	Bottom	180°	-0.057	-0.053	-0.052
Negative	180°	Top	0°	-0.066	0.021	0.021
	270°	Side	90°	0.445	0.449	0.449
Dipole	0°	Bottom	180°	-0.063	-0.056	-0.054

We have also inspected the influence of the host-guest binding on electronics structure. We have compared the bandgap values,  $\epsilon_{\text{bandgap}} = \epsilon_{\text{LUMO}} - \epsilon_{\text{HOMO}}$ , for the host, guest, and combined host and guest systems, as reported in Tables S1, S2. In both cases, the guest is aspirin. For

TNC, the following relations hold:  $\epsilon_{\text{guest bandgap}} > \epsilon_{\text{host bandgap}} > \epsilon_{\text{host+guest bandgap}}$ . However, for SC:  $\epsilon_{\text{guest bandgap}} > \epsilon_{\text{host+guest bandgap}} > \epsilon_{\text{host bandgap}}$ . Details on the electronic structure of host-guest complexes are

provided in **Figures S1-S2**. Examples of frontier orbitals for host-guest complexes are provided in **Figures S3-S4**.

We have found an interesting correlation between adsorption binding energy and bandgap energy. Specifically, the host-guest pairs, which have larger values of binding energy, provide a stronger change of bandgap upon binding. The correlations of binding and gap prompt a possibility to monitor the binding of host and guest by spectral probes.

## Conclusions

Our calculations show that through simple models, host-guest interactions of biologically relevant molecules

(e.g. aspirin) non-covalently binding to the building blocks of MOSCs can be determined. ESP maps allow us to predict possible binding sites on host molecules. Specifically, we were testing the hypothesis that negatively charged sites of the host preferentially bind with positively charged sites of guest, which accounts for the experimentally observed binding selectivity.<sup>6c</sup> In addition, the strongest adsorption on both sulfonylcalix[4]arene and the tetranuclear complex is observed for two configurations:  $\phi=\Theta=180^\circ$ ,  $d=3 \text{ \AA}$ , and  $\phi=180^\circ$ ,  $\Theta=0^\circ$ ,  $d=3 \text{ \AA}$ .

Adsorption energies of aspirin to TNC have low values  $-0.066 \text{ eV} < E(\text{bind}) < -0.052 \text{ eV}$ , corresponding to thermal quantum,  $KT \sim 0.027 \text{ eV}$ . Such weak binding can be broken by thermal fluctuations. The upper limit of strong hydrogen bond energy is generally considered to be about

1.8 eV. Nearly all bonding at  $3 \text{ \AA}$  of the SC occurs in this range, with the only exception being  $\phi=\Theta=0^\circ$ ,  $d=3 \text{ \AA}$ . This indicates that the binding of the aspirin to the SC is strong, but still able to be rinsed away, as is anticipated for such non-covalent host-guest interactions. Additionally, a dipole-dipole interaction is occurring here due to the permanent dipole moment that each host stand the guest maintain. Considering the strength of the dipole-dipole interactions, dispersion forces are less important.

Ongoing theoretical studies examine the building blocks and the MOSC as a whole, including structure, stability and binding energies of the MOSC host with various guest molecules. The adsorption mechanism of guest molecules to the various binding sites of the MOSC will be explored by *ab initio* molecular dynamics.<sup>23</sup> Additional experimental studies, with the guidance of these computational studies, will be performed, regarding guest selectivity to optimize the binding ability of the MOSCs. Once a thorough understanding of the binding capability of the MOSCs is complete, new guest molecules could be identified and the MOSCs could be modified in order to incorporate previously non-binding guests. The versatility of the MOSCs opens them up to a wide

range of applications, such as drug delivery vehicles and perhaps water treatment filters.

## References

1. Evans, W. E.; Relling, M. V., *Nature* 2004, 429 (6990), 464-468.
2. Noteboom, C.; Qureshi, S., *Health and Technology* 2014, 1 (4), 59-73.
3. Peer, D.; Karp, J. M.; Hong, S.; Farokhzad, O. C.; Margalit, R.; Langer, R., *Nat. Nanotechnol.* 2007, 2 (12), 751-760.
4. Kannan, N.; Vakeesan, D., *Renew. Sust. Energ. Rev.* 2016, 62, 1092-1105.
5. Peng, R.; Zhao, D.; Dimitrijevic, N. M.; Rajh, T.; Koodali, R. T., *The Journal of Physical Chemistry C* 2011, 116 (1), 1605-1613.
6. (a) Dai, F.-R.; Wang, Z., *J. Am. Chem. Soc.* 2012, 134 (19), 8002-8005; (b) Dai, F.-R.; Becht, D.C.;
7. Wang, Z., *Chem. Commun.* 2014, 50, 5385-5387; (c) Dai, F.-R.; Sambasivam, U.; Hammerstrom, A. J.; Wang, Z., *J. Am. Chem. Soc.* 2014, 136, DOI: 10.1021/ja502839b.
8. Morohashi, N.; Narumi, F.; Iki, N.; Hattori, T.; Miyano, S., *Chem Rev* 2006, 106 (12), 5291-5316.
9. Kajiwara, T.; Kobashi, T.; Shinagawa, R.; Ito, T.; Takaishi, S.; Yamashita, M.; Iki, N., *Eur J Inorg Chem* 2006, (9), 1765-1770.
10. Kitagawa, S.; Kitaura, R.; Noro, S. i., *Angewandte Chemie International Edition* 2004, 43 (18), 2334-2375.
11. Eddaoudi, M.; Moler, D. B.; Li, H.; Chen, B.; Reineke, T. M.; O'keeffe, M.; Yaghi, O. M., *Accounts Chem. Res.* 2001, 34 (4), 319-330.
12. Yaghi, O. M.; O'Keeffe, M.; Ockwig, N. W.; Chae, H. K.; Eddaoudi, M.; Kim, J., *Nature* 2003, 423(6941), 705-714.
13. Fischer, M.; Gomes, J. R. B.; Jorge, M., *Molecular Simulation* 2014, 40 (7-9), 537-556.
14. Gutsche, C. D., 2nd ed.; *The Royal Society of Chemistry: Cambridge, UK*, 2008.

15. Johnson, B. G.; Gill, P. M.; Pople, J. A.; Fox, D. J.,  
Chemical physics letters 1993, 206 (1), 239-246.
16. Dennington, R.; Keith, T.; Millam, J., Semichem  
Inc., Shawnee Mission KS 2009.
17. rimme, S., Journal of computational chemistry 2006,  
27 (15), 1787-1799.
18. Naray-Szabo, G.; Ferenczy, G. G., Chemical reviews  
1995, 95 (4), 829-847.
19. Brunold, T. C.; Conrad, K. S.; Liptak, M. D.; Park,  
K., Coord. Chem. Rev. 2009, 253 (5+6), 779-794.
20. Peter, L. M., Journal of Physical Chemistry Letters  
2011, 2 (15), 1861-1867.
21. Mora-Sero, I.; Bisquert, J., Journal of Physical  
Chemistry Letters 2010, 1 (20), 3046-3052.
22. Hodes, G., Journal of Physical Chemistry C 2008,  
112 (46), 17778-17787.